Fuel 294 (2021) 120316

Contents lists available at ScienceDirect

Fuel

journal homepage: www.elsevier.com/locate/fuel

Full Length Article

Evaluations of the feasibility of oil storage in depleted petroleum reservoirs through experimental modelling studies

Xinrui Zhao [a], Ridha Al-Abdrabalnabi [b], Yu-Shu Wu [a,*], Xianmin Zhou [b]

[a] Dept of Petroleum Engineering, Colorado School of Mines, USA
[b] College of Petroleum Engineering & Geosciences, King Fahd University of Petroleum & Minerals, Saudi Arabia

ARTICLE INFO

Keywords:
Oil storage
Energy security
Depleted petroleum reservoir
Storage capacity

ABSTRACT

The global storage space for crude oil is now facing intense challenges due to excess supply. In this situation, increasing oil storage capacity is urgently required. The currently available oil storage facilities, such as tanks and underground caverns, are of limited storage capacity, which cannot be expanded within a short time. Depleted petroleum reservoirs seem to be an ideal alternative since they are geographically ubiquitous and abundant, structurally safe, and cost-effective for storing large amounts of crude oil. Hence, this work aims to investigate the feasibility and approve the concept of oil storage in depleted petroleum reservoirs using both laboratory and modeling approaches. A core flooding experiment was conducted to physically model oil storage and withdrawal in a sandstone core. The results show that around 77% of the stored oil in the core is withdrawn. A core-scale model is then developed to match experimental data and collect inputs for the following studies. A sensitivity analysis is performed to determine the effect of porosity and permeability of the rock and bottom hole pressure (BHP) of the oil injectors on the storage capacity and withdrawal efficiency. The results demonstrate that the storage capacity increases with each of the parameters, but the withdrawal efficiency nearly holds constant. In the Field-scale modeling study, the reservoir stores 7.7 MMbbl oil, and the withdrawal efficiency are 67% and 74% for dead and live oil storage. It indicates oil storage in depleted reservoirs has a great potential to enlarge the global oil storage capacity.

1. Introduction

Oil storage serves many purposes, but its main objective is to contribute to energy security in the region [1,2]. In the last few decades, many countries have poured billions of dollars into developing such oil storage facilities. For example, China, now as one of the largest crude oil consumers, is using oil storage as the major means to reduce the impact of oil import cutoffs. Moreover, the U.S. Department of Energy (DOE) has mined more than 60 underground salt caverns to store emergency crude oil since 1977 [3,4]. These facilities now provide the world's largest emergency oil supply, known as the Strategic Petroleum Reserve (SPR).

There has been an increasing concern about the lack of storage space in recent years since the oversupply grows [4,5]. In 2020, members of OPEC and their allies agreed to cut the oil output in May and June. However, the situation has not been improved because the demand is continuously declining due to the global economic depression. Under such circumstances, the global storage space is under intense pressure since the unconsumed oil may eventually end up with oil storage. The expansion of the storage capacity is inevitable, however, hard to achieve relying on the existing storage facilities, such as oil tanks, floating storages, and underground caverns. Oil tanks and floating storages are expansive and need special care on corrosion to avoid leakage or seepage [6–10]. Underground salt caverns are a good alternative concerning safety and cost [11,12]. However, the storage capacity of storage caverns is restricted by the quantity of the local source rock [13]. Therefore, developing a new storage facility seems to be the best option to enlarge the global oil storage capacity.

The depleted petroleum reservoir is a potential oil storage facility considering its success in underground gas storage (UGS). Since the early 1960s, there have been operations of UGS using former gas and oil reservoirs [14]. After decades of relentless efforts, it has become a mature technique and the major surplus to the market requirements [15,16]. The depleted petroleum reservoir has certain advantages over other storage facilities. Firstly, they are abundant and geographically ubiquitous, thus possessing a larger storage space than any other storage

* Corresponding author. Tel.: +1 92 5330 3318.
E-mail address: ywu@mines.edu (Y.-S. Wu).

https://doi.org/10.1016/j.fuel.2021.120316
Received 16 October 2020; Received in revised form 18 January 2021; Accepted 23 January 2021
Available online 8 March 2021
0016-2361/

Table 1
Recipes of seawater.

Component	Concentration (g/L)
NaCl	41.041
$CaCl_2 \cdot 2H_2O$	2.384
$MgCl_2 \cdot 6H_2O$	17.645
Na_2SO_4	6.343
$NaHCO_3$	0.165
Total dissolved solids	57.670
NaCl	41.041
$CaCl_2 \cdot 2H_2O$	2.384
$MgCl_2 \cdot 6H_2O$	17.645
Na_2SO_4	6.343

Table 2
Fluid properties (measured at 25 °C).

Fluid	Density (g/cc)	Viscosity (cP)
Seawater	1.0385	0.972
8% NaI seawater	1.0933	0.974
Dead Crude Oil	0.8704	12.49
Seawater	1.0385	0.972

facility [17]. Secondly, these primordial reservoirs are usually structurally stable, minimizing the hazard and risk associated with subsurface oil storage [18]. Lastly, converting an oil field from production to storage takes benefits from the existing wells, pipelines, and other facilities, making it cost-effective. Even these advantages have been noticed for many years, the concept of using a depleted reservoir to store crude oil has not been proven yet. Thereby, in this work, oil storage feasibility in depleted petroleum reservoirs is systematically investigated through experimental and modeling studies.

In order to evaluate the concept proposed in this study, the storage capacity and recovery efficiency of the stored oil need to be analyzed. Compared with a storage tank or storage carven, a depleted reservoir's storage capacity is generally large but maybe hard to quantify analytically. During the operation, the oil is injected through existing producers or injectors, forcing the pre-existing fluid away from these wells to create space for oil storage. Such a process involves the fluid flow in porous media and expansion or compression of the fluid and rock. Therefore, for a depleted reservoir, the storage capacity depends on many factors, such as injection pressure, permeability, porosity, and formation heterogeneity [19]. The recovery efficiency of the stored oil may also vary from case to case due to the reservoir heterogeneity, nonuniformity, and properties of crude oil. The injected water used for the withdrawal of the stored oil has a preference to go through high permeability zones, bypassing some of the stored oil [20]. For this reason, the recovery efficiency will always be less than 100%.

In consequence, the numerical approach turns out to be the best way to evaluate these two parameters. In this study, three numerical models on different scales are built using a black oil simulator. To better understand the underlying physical processes of the proposed oil-storage concept and collect critical inputs for modeling studies, laboratory tests were also carried out.

2. Experimental work

2.1. Fluids

In the laboratory study, seawater, 8% NaI seawater, and crude oil from a carbonate reservoir were used as a displacing and displaced

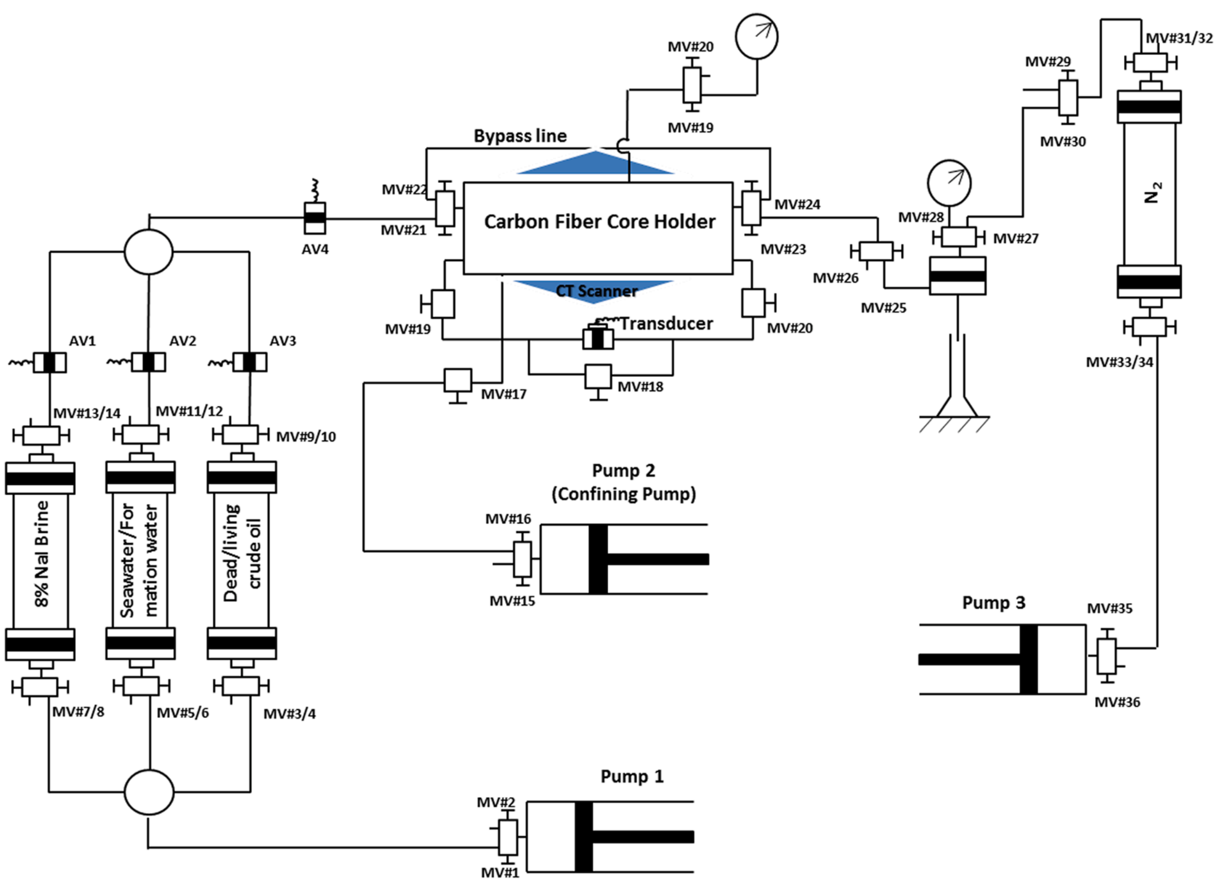

Fig. 1. Flow chart of the experimental setup.

phase. The components of seawater are listed in Table 1. The viscosity and density of fluids were measured at 25 °C using the SVM 3001 apparatus, as listed in Table 2.

2.2. Core plug

The strongly water-wet Berea sandstone core plug with a dimension of 6″ in length and 1.5″ in diameter, ZW-B-1, was used for the core flooding experiment. The core plug was cleaned with toluene and methanol by a Soxhlet extractor. The core plug's dry and wet weight was recorded before and after saturating the core with 8% NaI seawater to determine the pore volume (PV) and porosity of the core based on material balance. The core was then placed into a vessel filled with 8% NaI seawater for ten days to establish ionic equilibrium at ambient conditions. It was then loaded into an X-Ray core holder connected to a core flooding apparatus to measure brine permeability and future use. The brine permeability and porosity of the core plug were 76.5 mD and 18.56%, respectively. The pore volume of the core plug was 32.07 cc.

2.3. X-Ray core flooding apparatus

The core flooding setup is shown in Fig. 1 in which includes a carbon fiber X-Ray core holder, two injection pumps, several transducers to measure the inlet and outlet pressure and differential pressure, a confining system incorporating an injection pump and a transducer to measure confining pressure; an acoustic separator for the separation of water and oil, a back pressure regulator, three floating piston accumulators filled with 8% NaI seawater, seawater, and oil, an oven to adjust the constant temperature, a data acquisition system (DAC) for the collection of the information from X-ray scanner and core flooding system. The test conditions were set up at pore pressure of 500 psi, confining pressure of 1500 psi, and temperature of 25 °C for initial and second water flooding.

2.4. Experimental procedure

2.4.1. Establishment of first initial water saturation, S_{wi1}, by crude oil injection (Forced drainage imbibition)

After brine permeability was measured, the oil was injected into the core at elevated injection rates ranging from 0.0 to 1.2 cc/min to displace water at experiment conditions of a confining pressure of 1500 psi and temperature of 25 °C. Based on the water production and the injection pressure during such a process, the initial water saturation (S_{wi}) and original oil in the core (S_{oi}) can be calculated. The forced drainage capillary curve, injection pressure (P_{c1}) vs. water saturation (S_w), can also be obtained. Totally 56 PV of crude oil was injected for the forward flow and 9 PV for reverse direction flow to reduce the capillary effect. Other parameters, such as original oil in the core (OOIC) and oil permeability at S_{wi1}, $K_{o(Swi1)}$, were also calculated based on the raw data obtained during crude oil injection.

2.4.2. First water flooding (1st WF):

After establishing the S_{wi} and S_{oi}, 8% NaI seawater was injected into the core plug at a confining pressure of 1500 psi and pore pressure of 500 psi to displace oil. The testing temperature was set to 25 °C. Multiple injection rates (0.1, 0.25, 0.5, and 1.0 cc/min) were applied for water injection to reach the water-flooded residual oil saturation. When no more oil was produced from the outlet or 99% of the water cut was reached, water injection ended. The oil production, water production, and differential pressure across the core were recorded with elapsed time. Several scans were performed during water flooding to monitor oil and water saturation distributions inside the core plug. The characteristic parameters, such as maximum water saturation, $S_{w(max)}$, residual oil saturation, S_{orw1}, water permeability at S_{orw1}, $K_{w(Sorw1)}$, were calculated based on the raw data for first water flooding.

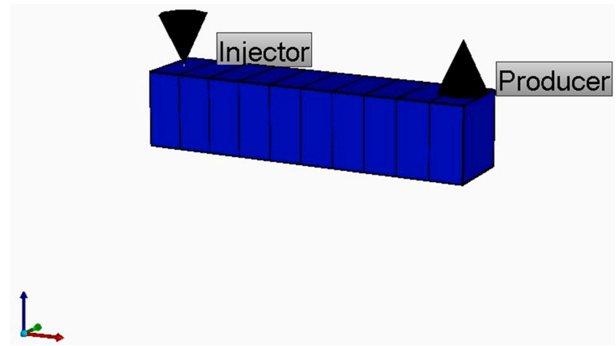

Fig. 2. Special discretization of the 1-D rectangular core-scale model.

Table 3
Input parameters for the core-scale model.

Parameter	Value
Reservoir temperature, °F	77
Stock tank oil density, Lb/ft^3	54.3373
Gas gravity (Air = 1)	0.7
Water phase density, Lb/ft^3	68.2523
Formation volume factor	1.01333
Water viscosity, cp	0.972
Initial oil saturation, %	80
Residual oil saturation, %	40
Oil relative permeability at connate water saturation	0.8
Water relative permeability at residual oil saturation	0.3

2.4.3. Establishment of second initial water saturation, S_{wi2} by second crude oil injection (second forced drainage imbibition)

By the end of first water flooding, residual oil, as the non-mobile phase, and water, as the mobile phase, are in the core plug. The reinjection of crude oil was conducted at 0.1 cc/min, and the testing conditions were consistent with that in the 1st WF. The reinjection was stopped until no more water producing from the core plug, and thereby S_{wi2} can be determined by the material balance method or the X-ray scanner. The second oil saturation (S_{oi2}), oil permeability at S_{wi2}, $K_{o(Swi2)}$, etc., were calculated based on the raw data obtained at the end of the second crude oil injection. The second forced drainage capillary curve, injection pressure (P_{c2}) vs. water saturation, can be plotted as well.

2.4.4. Second water flooding (2nd WF):

After the establishment of S_{wi2} and S_{oi2}, we conducted the second water flooding, which injects water into the core to displace oil at injection rates of 0.1, 0.2, and 0.4 cc/min. The testing procedure of the 1st WF was applied here. The characteristic parameters of 2nd WF, including maximum water saturation, $S_{w(max)2}$, remaining oil saturation, S_{orw2}, water permeability at S_{orw2}, $K_{w(Sorw2)}$, etc., were calculated based on raw data obtained during the 2nd WF.

3. Numerical modeling studies

3.1. Core-scale model for history matching

To evaluate the possibility of utilizing a depleted petroleum reservoir to store crude oil, we first established a one-dimension rectangular, core-scale model developed using the black oil model in CMG's IMEX to match the experimental data. As shown in Fig. 2, the core-scale model kept the cross-section area identical to that of the cylindrical core for consistency. There were 10 grids in I direction, the flow direction, and one grid in J and K direction. An injector and a producer were located in the first block and tenth block, severally, representing the core holder's inlet and outlet. The input parameters, such as rock data, fluid data, and

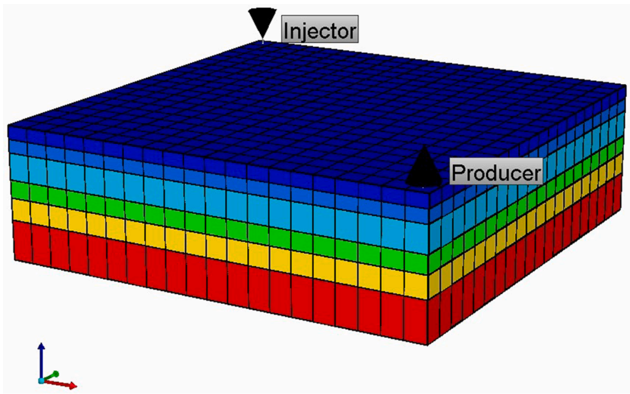

Fig. 3. Spatial discretization of the homogeneous model.

Table 4
Geological data for the simple shoe-box model. Grid top at 2000 ft.

Layer	Thickness	Permeability (I), mD	Permeability (J), mD	Permeability (K), mD	Porosity
1	30	250	250	180	0.3
2	100	300	300	320	0.3
3	60	230	230	160	0.3
4	40	200	200	60	0.3
5	50	300	300	240	0.3
6	20	100	100	80	0.3

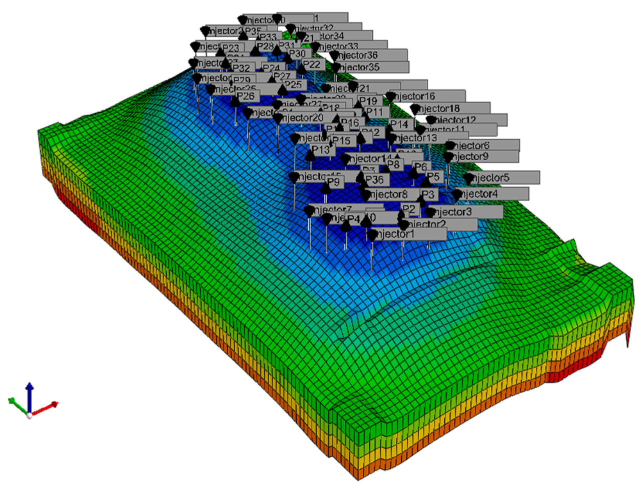

Fig. 4. Spatial discretization of the field-scale model. Grid top at 2000 ft.

rock-fluid interaction data, used in the base case, were completely consistent with the experimental data, as presented in Table 3. The gas-oil ratio was set to a particularly low value to avoid the presence of the free gas. The inputs were tuned to achieve the best match of the target outputs, recovery factor (RF) of the oil, and differential pressure. Thus, the model can accurately represent the core flooding experiment. These tuned input parameters will be used to establish other models followed in this study.

3.2. Simple shoe-box numerical model for sensitivity analysis

The sensitivity analysis employed a shoe-box numerical model with a water injector and producer along the diagonal, aiming to represent one-fourth of the five-spot pattern. This model has an areal dimension of 1000 × 1000 ft and a vertical length of 300 ft. It was discretized into 20 × 20 cells in the areal section and 6 cells in the vertical section, as shown in Fig. 3. Each layer was given different thicknesses and permeabilities to create heterogeneity, which is listed in Table 4. The fluid properties, such as density and viscosity, were updated according to this model's reservoir temperature (77 °F). The workflow is described as follows: the injector and producer were open under constant BHP for 10 years to deplete the reservoir; then the oil was injected at a constant injection pressure from an oil injector, which overlaps the producer for six months; after two years of storage, the water injector and the producer were resumed to withdraw the stored oil. The sensitivity analysis above was conducted with dead oil as the stored oil.

Table 5
Geological setting of the field-scale model.

Layer	Thickness	Permeability (I), mD	Permeability (J), mD	Permeability (K), mD	Porosity
1	90	250	250	105	0.17
2	80	190	190	87	0.16
3	80	220	220	96	0.25
4	70	240	240	102	0.14

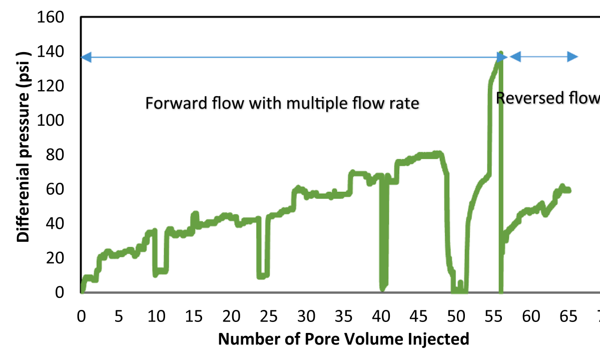

Fig. 5. Differential pressure vs. pore volume injected during initial oil injection with multiple injection rates.

3.3. Field-scale modeling study

To simulate the oil storage behavior in field applications, a field-scale model with 45 × 90 × 4 cells was created, as shown in Fig. 4. It includes 51 injectors and producers, respectively, located according to the five-spot pattern. The model was made to have an anticline shape, where the oil–water contact was at 2000 ft. An aquifer was added at the bottom of the reservoir. The total pore volume of the reservoir was around 590 MMbbl. Further geological settings can be found in Table 5. The input parameters and operating procedures were kept consistent with the sensitivity analysis. The primary constraint was constant BHP for both injectors and producers. The maximum injection capacity and deliverability of wells were set to 8000 bbl/D and 10,000 bbl/D, respectively.

4. Results and discussion

4.1. Core flooding experiment

4.1.1. Initial crude oil injection (forced drainage process)

The purpose of injecting crude oil into the core is to simulate water migration in the reservoir by oil generation in the source rocks and obtain the forced drainage capillary curve. The characteristic parameters, S_{wi} and S_{oi}, can be calculated using material balance when about 56 PV oil from the forward direction and 9 PV from the reversed flow direction were injected into the core at ambient condition. The different pressure changes with the elevated injection rate, as presented in Fig. 5. By the end of the oil injection, S_{wi} and S_{oi} of the core plug reached 21.27% and 78.73%, respectively. The oil permeability at initial water saturation was 17.44 mD. The relationship between injection pressure

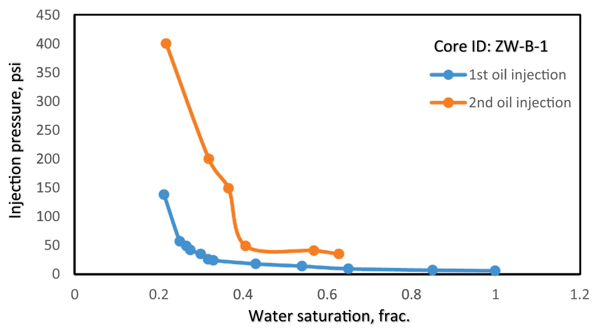

Fig. 6. The relationship between injection pressure and water saturation during forced drainage process of first and second oil injection (Core ID: ZW-B-1).

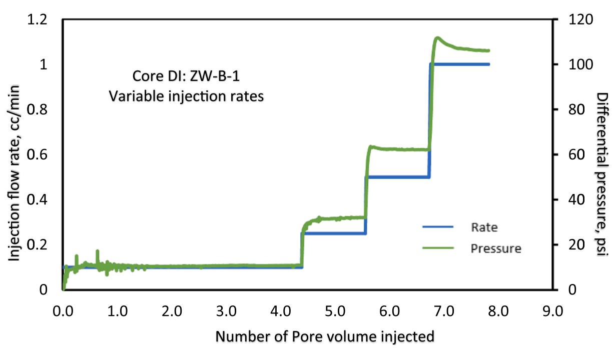

Fig. 7. Differential pressure along with the core and the injection rates vs. injection volume during first water flooding.

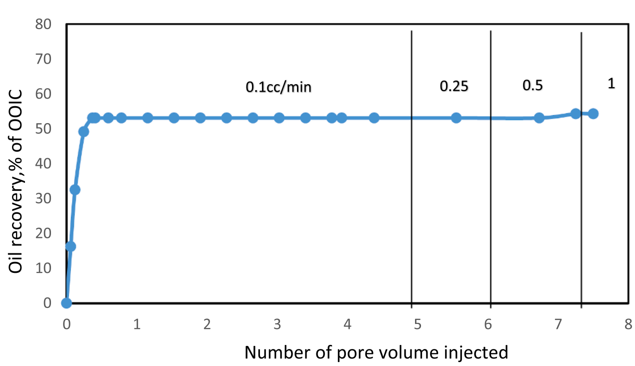

Fig. 8. Oil recovery vs. injection volume for first water flooding.

and water saturation has been shown in Fig. 6.

4.1.2. *Experimental results from first water flooding*

Fig. 7 shows the differential pressure and injection rate vs. the injection volume during first water flooding. The water breakthrough occurs when about 0.4 PV was injected. The corresponding oil recovery at breakthrough is about 53% of OOIC, as shown in Fig. 8. After that, no more oil is produced at an elevated injection rate until reaching 1.00 cc/min. About 1% of oil recovery was recovered at 1.00 cc/min and the final oil recovery was around 54% of OOIC. Table 6 summarizes the characteristics parameters of first oil injection and oil recoveries and dynamic parameters of first water flooding.

4.1.3. *Second crude oil injection (second forced drainage process) for the establishment of second initial water and original oil saturation*

After the 1st WF, the oil was reinjected into the core to establish S_{wi2} and S_{oi2} with a pore pressure of 500 psi and an injection rate of 0.1 cc/min. The experimental procedures were kept consistent with that for the first oil injection. During oil reinjection, 13.25 cc of water was produced when around 6.3 PV of crude oil was injected into the core plug, which means an equal volume of oil injected into the core. Comparing the differential pressure profiles between the first and second oil injection, we found that the differential pressure for the second oil injection process is much greater than that for the first oil injection, as shown in Fig. 6. Unlike the first oil injection, the core here fills not only with water but also oil. In this strongly water-wet sandstone core, the displacement and capillary forces are the driving force of oil displacement. Capillary forces mostly decide the amount of the remaining oil between water and oil [21]. Such a capillary force creates a great resistance for oil to flow through the core, thus resulting in higher injection pressure. S_{wi2}, S_{oi2}, and $K_{o(Swi2)}$ are listed in Table 6.

Table 6
Summary of dynamic parameters and oil recoveries for core flooding experiment.

Initially, characteristic parameters of the core at the end of the first oil flooding		
Initial water saturation, S_{wi}:	21.27	% of PV
Initial oil saturation, S_{oi}:	78.73	% of PV
The pore volume of core:	32.07	cc
Original oil in core:	25.25	cc
Oil permeability at original oil in core:	17.44	mD
Dynamic parameters after first water flooding		
Oil production by WF:	13.4	cc
Oil recovery at BT:	53.07	% of OOIC
Final Oil recovery:	54.3	% of OOIC
Endpoints for first water flooding		
Residual oil saturation, S_{or1}:	36	% of PV
Max water saturation, $S_{w(max)}$:	64	% of PV
Brine permeability at S_{or1}: Kw(S_{or1}):	2.8	mD
Second characteristic parameters of the core at the end of second oil flooding		
2nd-initial water saturation, S_{wi2}:	22.8	% of PV
2nd-Initial oil saturation, S_{oi2}:	77.2	% of PV
The pore volume of core:	32.1	cc
Original oil in core:	24.8	cc
Oil permeability at S_{wi2}:	1.33	mD
Dynamic parameters after second water flooding		
Oil production by WF:	10.3	cc
Oil recovery at BT:	30	% of OOIC
Final Oil recovery:	41	% of OOIC
Endpoints at second water flooding		
Residual oil saturation, Sor2:	45.21	% of PV
Max water saturation, Sw(max)2:	54.79	% of PV
Oil permeability at Sor2:	0.29	mD
Re-recovery oil based on reinjection of oil after first water flooding		
Reinjection oil volume in core:	13.3	cc
Oil production by 2nd WF:	10.3	cc
Oil recovery:	77.4	% of 2nd OIC

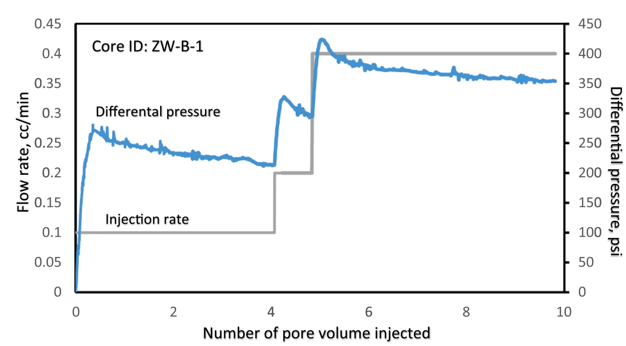

Fig. 9. Differential pressure along with the core and the injection rate vs. injection volume during second water flooding.

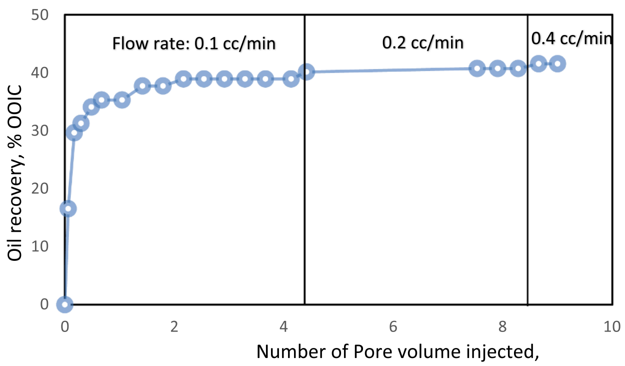

Fig. 10. Oil recovery vs. pore volume injected during second water flooding (oil recovery calculated based on second OIC.

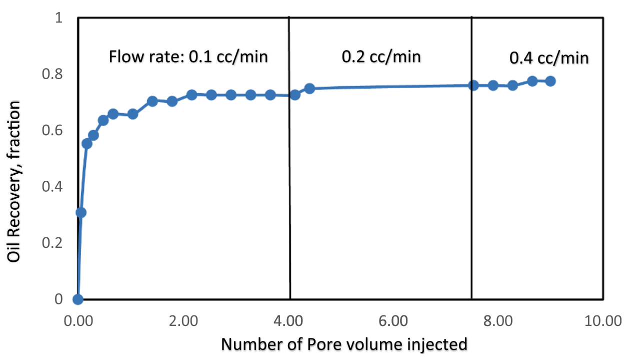

Fig. 11. Oil recovery efficiency (RE) vs. pore volume injected during the second water flooding (Oil recovery efficiency calculated based on the volume of oil reinjected into core).

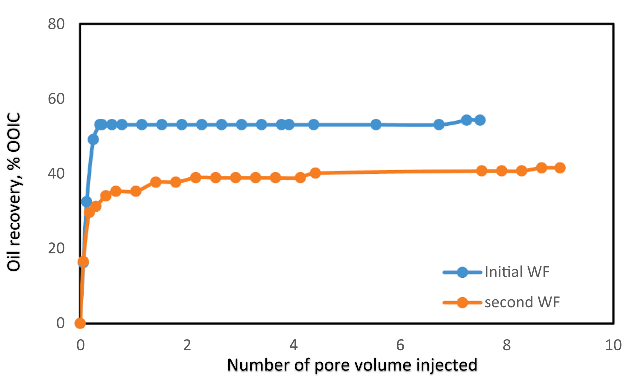

Fig. 12. Comparison of oil recoveries between initial and second water flooding.

4.1.4. Experimental results from second water flooding

The 2nd WF was performed at the same testing conditions as the 1st WF, but with different injection rates. As shown in Fig. 9, the water breakthrough occurred when 0.4 PV of water was injected, which is similar to that of the 1st WF. When the flow rate increases, the injection pressure increases correspondingly and then gradually declines. By the end of the 2nd WF, RF is about 42% OOIC, or 77% of stored oil, as shown in Figs. 10 and 11, respectively. To avoid confusion, we will call the stored oil RF as refer to recovery efficiency (RE) from here on. Comparing the 1st and 2nd WF, the results are quite different in two aspects. Firstly, the differential pressure of the 2nd WF is much greater than that of the 1st WF. Then, RF is lower in the 2nd WF as described in Fig. 12. A possible reason for these phenomena is that the wettability of the core changed during the second oil injection, reducing the relative

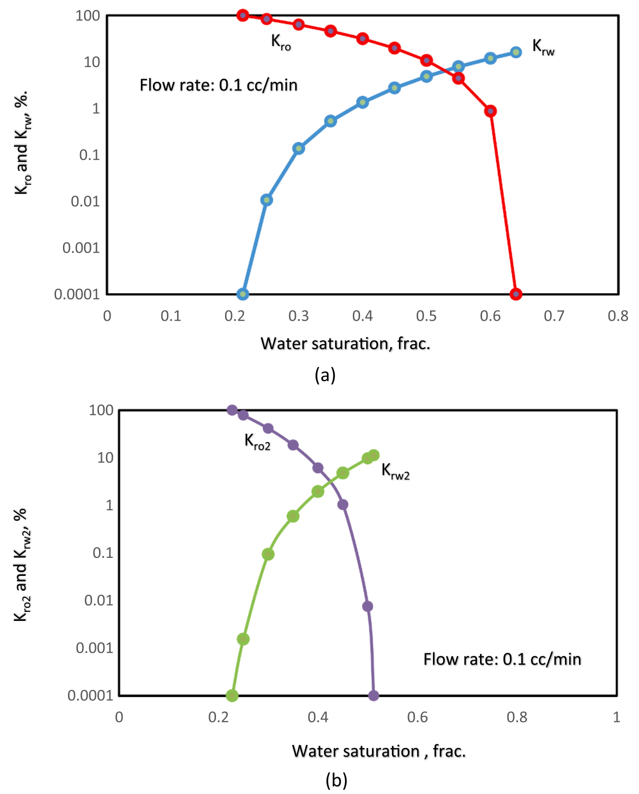

Fig. 13. Relative permeability curves of the first (a) and second (b) water flooding.

permeability to water [22]. To better understand this phenomenon, the water and oil relative permeability curves of the 1st and 2nd WF were computed using Corey's model [23], as described as follows:

$$K_{rw} = K_{rw(Sorw)}(S)^{N_w} \tag{1}$$

$$K_{ro} = K_{ro(Swi)}(1 - S)^{N_o} \tag{2}$$

$$S = \frac{S_w - S_{wi}}{1 - S_{wi} - S_{orw}} \tag{3}$$

Where N_W and N_o are 3 and 2 for the 1st WF, and 3 and 3.3 for the 2nd WF, according to the literature [24].

Fig. 13(a) shows the relative permeability vs. water saturation during the 1st WF. The intersection of two curves occurs at the water saturation of 53%, which represents a typical relative permeability curve of displacing oil by water in a water-wet system. For the 2nd WF (Fig. 13(b)), the intersect shifts to the left, indicating wettability change. When oil injection lasts long enough, or the injection volume reaches a certain level, such a process is equivalent to aging the core with crude oil, eventually altering the rock wettability.

4.2. Numerical study

4.2.1. Core-scale model

The history matching of oil RF and differential pressure for 1st WF was completed, as shown in Fig. 14. The simulated differential pressure matches the experimental data using the primary inputs. However, the RF cannot match the experimental result for the first time, thus requiring an adjustment of the input parameters. The relative permeability curves were tuned primarily to match the RF.

For simulating the second oil injection process, the water injector was shut down, and the oil injector set at the same position was opened to inject oil. At the end of the second oil injection, S_{wi2} is around 23.08%.

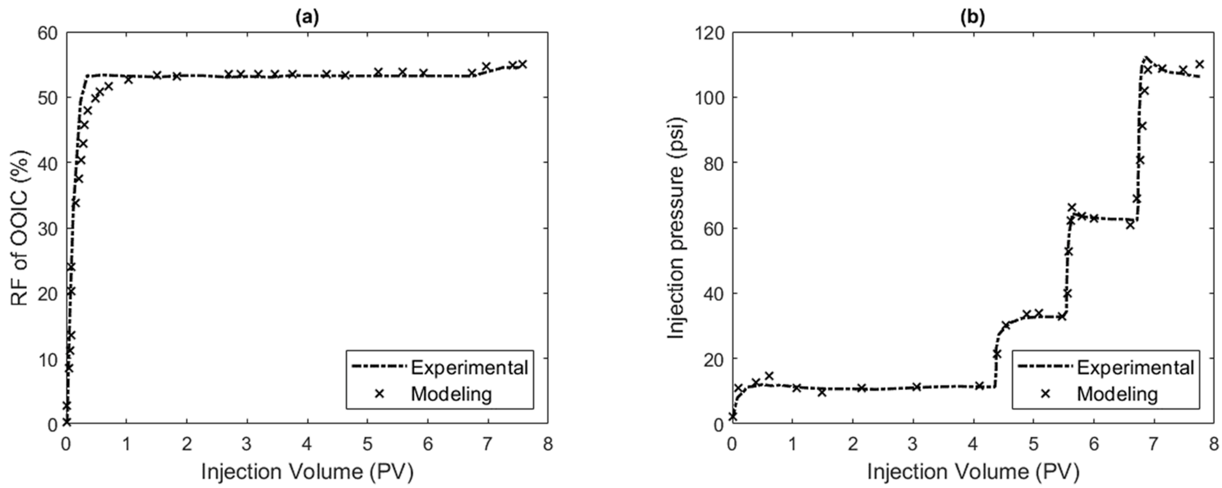

Fig. 14. Matching RF (a) and differential pressure (b) during the first water flooding.

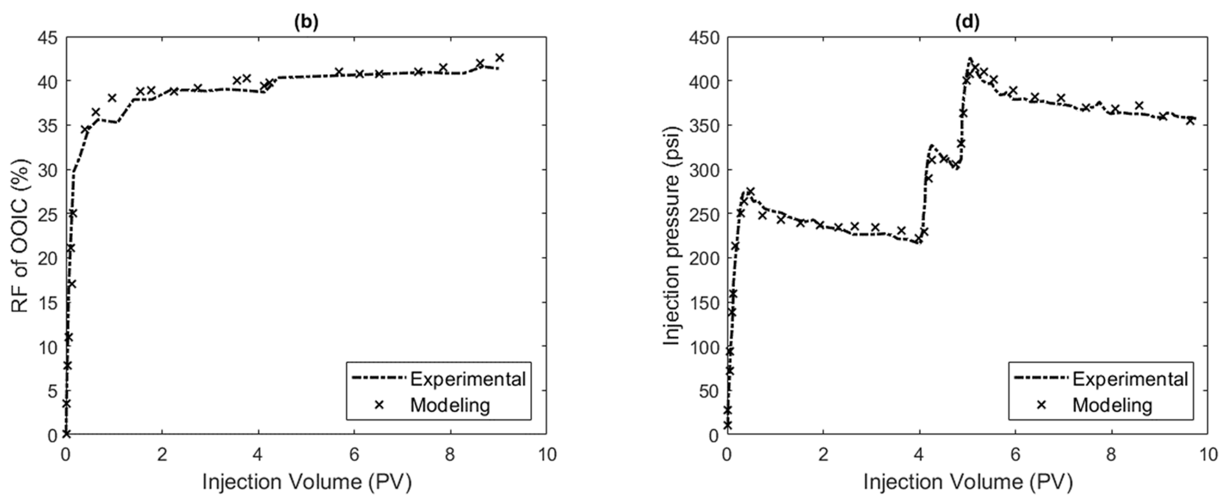

Fig. 15. Matching RF (a) and differential pressure (b) during second water flooding.

In the 2nd WF, the rock type was changed to oil-wet, and the relative permeability curves were modified accordingly. Similarly, the relative permeability curve was slightly tuned to match the RE and differential pressure, as presented in Fig. 15.

4.2.2. Sensitivity analysis using shoe-box model

After validating the core-scale model through history matching, those adjusted input parameters were used in the shoe-box model to conduct the sensitivity analysis for the effect of BHP, porosity, and permeability of the rock. This model is larger than the core-scale model and introduces heterogeneity to the porous medium. An injector and a producer were placed at the two ends of the diagonal, respectively, as referring to the five-spot waterflooding pattern. Note that this study did not consider the wettability change due to the smaller injection volume and short storage period. In the lab experiment, more than 6 PV of oil was injected to establish S_{wi2}, which was inapplicable to the field operations. The stored oil only occupied a small portion of the reservoir. During the injection of storage oil, there are no producers that enable the production of any fluids. Consequently, the injected oil will force the pre-existing fluid to flow elsewhere in the reservoir, taking the region near the producers. The injection pressure, reservoir porosity, and permeability play important roles in such a process. The impacts of these parameters on oil storage behavior are discussed as follows.

4.2.2.1. Bottom hole pressure (BHP). As shown in Fig. 16(a), the injection volume increases with an increase in BHP. Typically, BHP has no significant influence on an underground storage carven's storage capacity since it consists of an empty confined space with impermeable boundaries, and dead oil is hardly compressible. Depleted reservoirs, however, are permeable and fills with fluids such as water and remaining oil. At higher injection pressure, the injected fluid is more capable of propagating through the porous medium and pushing the pre-existing fluid away from the injection wells, which eventually enlarges the storage capacity [25].

Fig. 16(b) shows the change in RE during the five-year withdrawal with different BHPs. The RE of store oil increases dramatically during the first six months and then increases slightly as the production continues. The differences in the RE for these five cases are considerably small since the curves almost overlap each other. It indicates that the BHPs have a minimal impact on the RE. For field applications, one should only consider the RE in the desired time interval (6 months in this case as represented by the dashed line), taking into account the operating cost. Thus, Fig. 16(c) was computed to observe the difference in RE at six months. It demonstrates that the RE decreases with an increase in the BHP. However, the difference between RE's data point is below 0.003, which is too small to influence the oil storage applications. Therefore, increasing BHP is beneficial for oil storage applications since it brings greater storage capacity. Note that BHP should fall within a

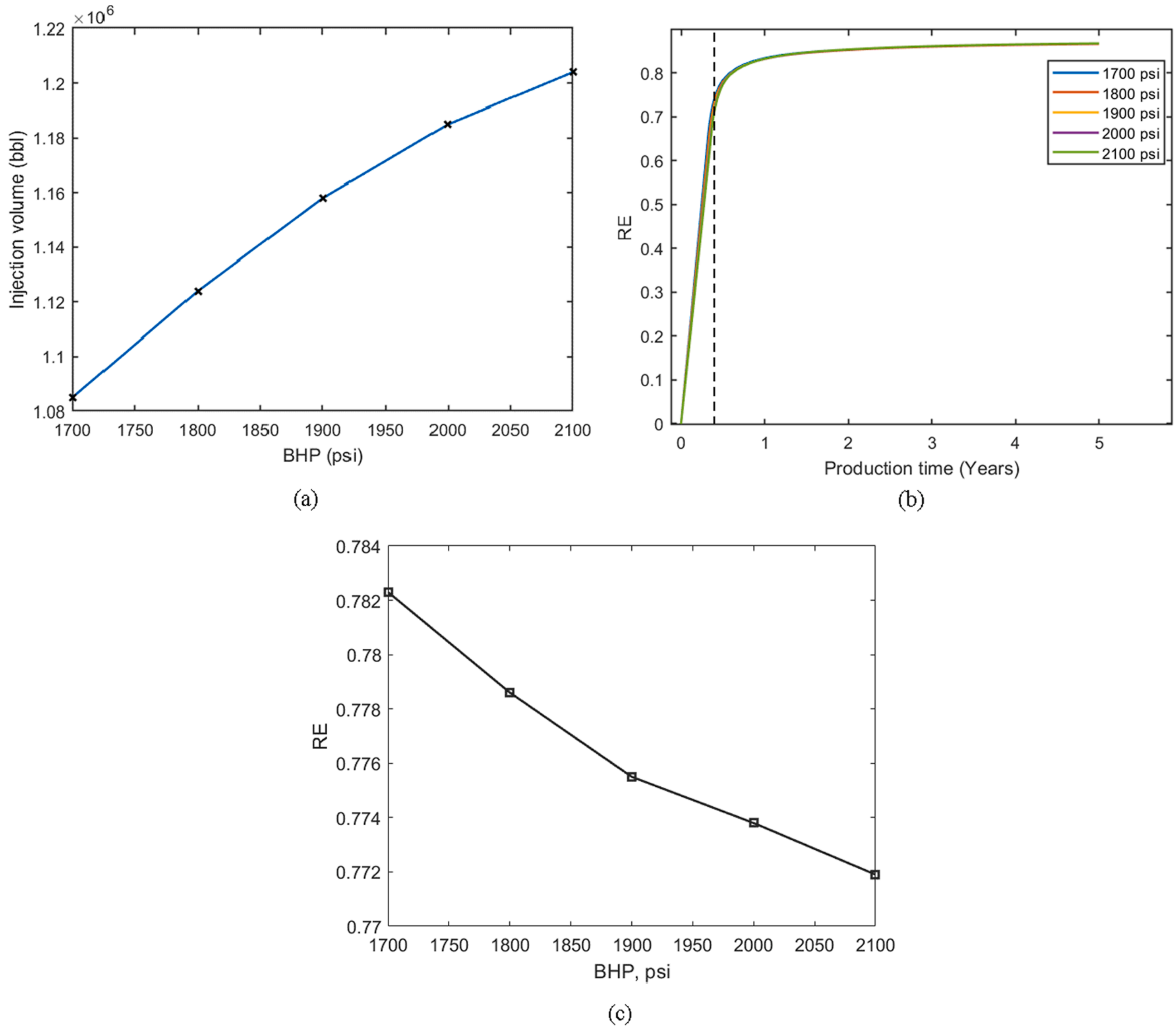

Fig. 16. (a) Injection volume, (b) Recovery efficiency over five-year withdrawal, and (c) recovery efficiency when withdrawal time equals six months with various BHPs.

certain range to avoid the breakdown of the formation. Operators must consider the formation breakdown pressure and the safety factor before decision making [26].

4.2.2.2. Porosity of the rock. Considering that the porosity of a depleted petroleum reservoir characterizes the volume of the void space in a rock, it appears to be the dominant factor for evaluating the oil storage candidates. In the case of a uniform and homogeneous porous medium, the storage capacity of the reservoir supposes to be proportional to the porosity. In this heterogeneous reservoir, the relationship between a rock's storage volume and porosity is positive but nonlinear, as shown in Fig. 17(a). As a result of the reservoir heterogeneity, the injected fluid has a preference to go through the high permeability zones leading to an uneven distribution of the stored oil. However, the porosity of the rock still has a considerable impact on the storage capacity. The effect of porosity of the rock on RE is not notable during the first six months; however, it became more significant as the production continues (Fig. 17(b)). When comparing the REs at six months of production, it shows a bell-shaped curve (Fig. 17(c)), where the peak of the RE appears at the porosity of 0.3. Still, the difference is too small to affect oil storage applications.

4.2.2.3. Permeability of the rock. The permeability of the reservoir affects both the storage capacity and the RE of storage oil since it controls the propagation of the fluid. When the base case's permeability decreases by 10% each time (up to 40%), the injection volume reduces accordingly, as shown in Fig. 18(a). However, the impact of the permeability on the RE is fairly small. In Fig. 18(b), the five curves are difficult to distinguish until the withdrawal time reaches three years. In Fig. 18(c), the maximum and minimum RE difference is only about 0.015. The small differences in the RE are caused by the high permeability of the base case. The reservoir permeability is still favorable for oil to flow even after being reduced. Certainly, one can decrease the permeability to a low level (several mD or even less) to increase the difference in the RE for comparison purposes. However, such a low permeability environment is not suitable for underground oil storage and is not considered in this study.

4.2.3. Field-scale model

In the above section, around 75% to 80% of stored oil can be withdrawn to the ground in six months. However, for field applications, this number may be much lower due to the reservoir's heterogeneity, structural complexity, and reservoir size. Hence, a field-scale model with

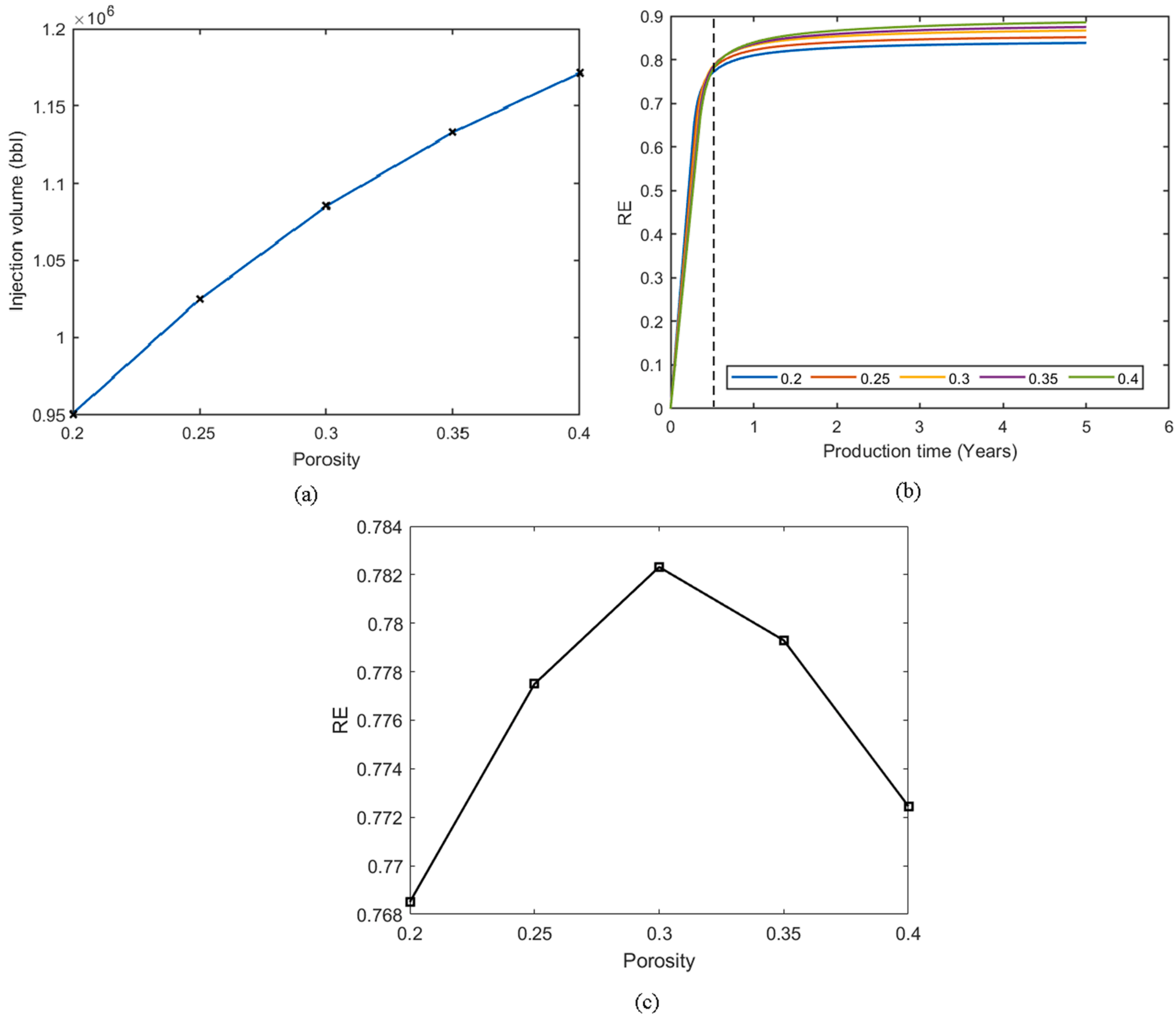

Fig. 17. (a) Injection volume vs. porosity of the rock, (b) Recovery efficiency vs. five-year withdrawal with different porosities, and (c) recovery efficiency when withdrawal time equals six months vs. various porosities.

an anticline shape was developed to evaluate the storage behavior more realistically. According to Fig. 19, we can understand how the oil saturation change in the reservoir during an oil storage operation. After 30 years of production, there is no oil produced by water flooding, which demonstrates the depletion of the reservoir. Around 77 MMbbl oil was then injected into such a reservoir from the oil injectors that overlap the producers in six months. Only a small fraction of the reservoir, mostly the region near the producers, occurs significant oil saturation change. Even so, such a reservoir still holds seven times the storage capacity of a typical salt cavern (10 MMbbl). During the production period, around 67% of the stored dead crude oil is withdrawn in six months, as shown in Fig. 20, which is, as expected, lower than the number in the sensitivity analysis. It is worth noting that this model is still ideal for representing a natural reservoir in terms of reservoir heterogeneity. A natural reservoir usually contains many high-permeability channels, leading to the low sweep efficiency of the injected water. Hence this model may overestimate the RF of the initial oil in place to a certain extent. However, the withdrawal efficiency of the stored oil can still be accurately predicted by this model due to the following: (a) The stored oil only occupies a small area close to the well and cannot penetrate deep into the reservoir, which weakens the effect of reservoir heterogeneity significantly. (b) Since the stored oil is injected into the reservoirs through wells, the majority of them flow through the high-permeability channels and stay there until being displaced by the injected water. In such cases only a tiny amount of stored oil that diffuse into the matrix will be bypassed by the displacing water.

As seen from Fig. 20, with the continuation of oil production, there is still a considerable amount of oil that can be withdrawn. It demonstrates that if the withdrawal rate increases by any means, more oil can be produced in the same period. The method of increasing the water injection rate is the most direct way; however, it may meet limitations in the field application. Injection of live oil seems to be an effective way since the dissolved gas expands to provide additional energy support during the production period. Besides, the oil swelling and viscosity reduction are also beneficial for the oil withdrawal. As a result, a simulation run was conducted using live oil as the stored fluid. In CMG's IMEX, there is no option to inject live oil directly. So, gas injectors were added in the positions of each oil injector. The gas injection was designed carefully according to the gas-oil ratio at reservoir conditions, ensuring no free gas existed in the reservoir. The oil injection volume (75 MMbbl) is still slightly lower than that of the former case due to the solution gas. However, this time, the RE at six months increases to 74%, as shown in Fig. 21. With the aid of other techniques such as artificial lift, the RE may further improve.

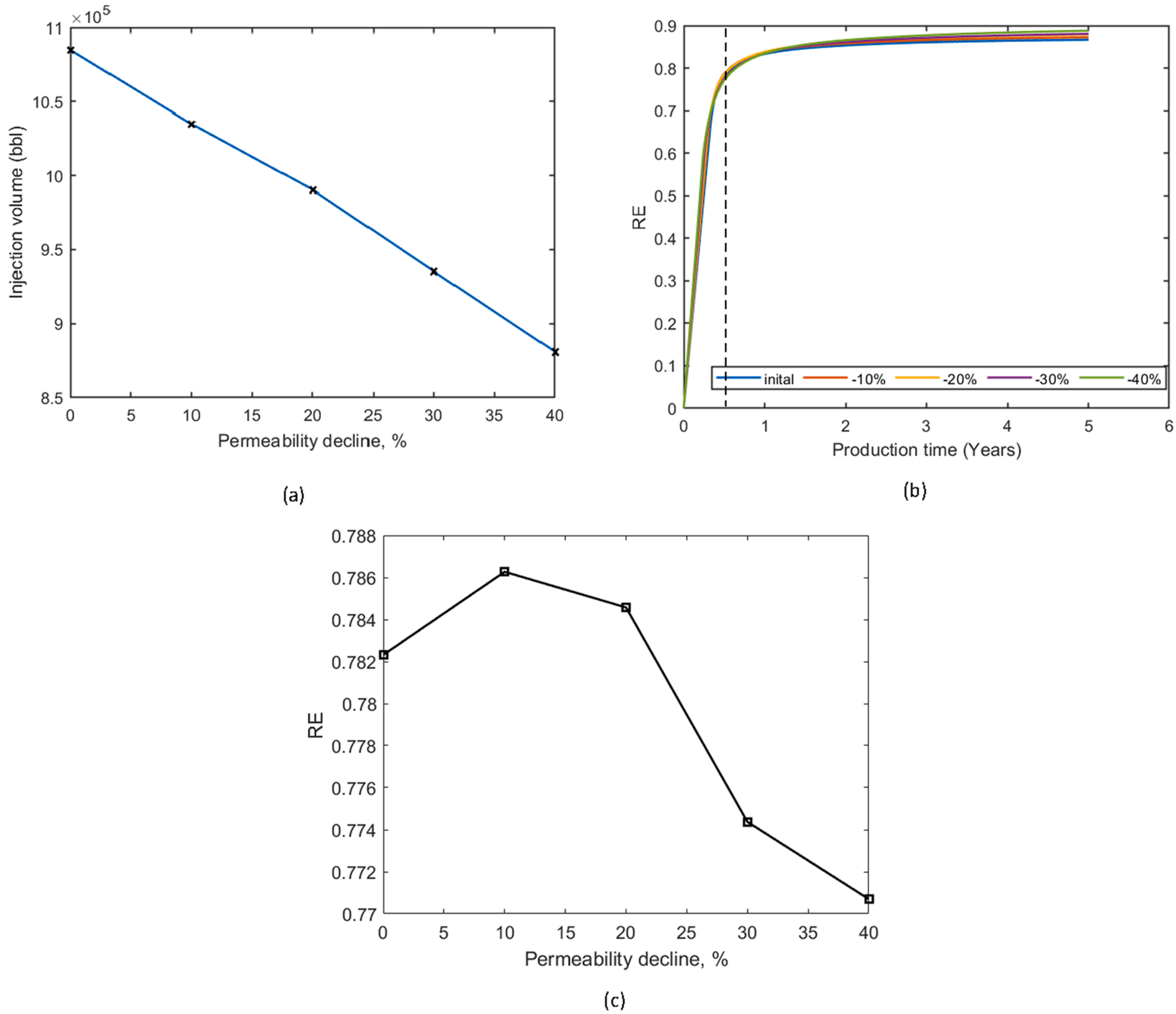

Fig. 18. (a) Injection volume vs. permeability decline, (b) Recovery efficiency vs. five-year withdrawal with different permeability decline, and (c) recovery efficiency when withdrawal time equals six months vs. different permeabilities.

5. Concluding remarks

This paper presents a systematic study on the feasibility of oil storage in a depleted petroleum reservoir using laboratory tests and modeling approaches. To the best of our knowledge, this is the first attempt to examine this concept in the literature. Core flooding tests are accomplished to obtain the input parameters for numerical models and evaluate their oil-storage behavior. It shows the wettability changes from strongly water-wet to slightly oil-wet during oil injection, and the RE is about 77%. In the core-scale modeling study, the numerical results match the experimental results after tuning the relative permeability curves. The sensitivity analysis result shows the storage capacity is highly dependent on BHP, permeability, and porosity, while RE is barely affected by these parameters. In the field-scale modeling study, the reservoir stores 7.7 MMbbl oil, which is seven times the storage capacity of a typical salt cavern. The RE of dead crude oil is around 67%. In the case of live oil storage, the RE increases to 74%.

A depleted petroleum reservoir has a huge advantage over other existing storage facilities from a storage capacity perspective. Based on modeling results in this study, a depleted reservoir can hold several times or even dozens of times the storage capacity of a typical salt cavern, depending on the reservoir size. Besides, these reservoirs are geographically ubiquitous and plentiful, making it a good option to enlarge the global storage space.

Even RE is comparatively low from an economic standpoint, and the low operating cost still allows it to be commercially viable. Hence, a conclusion can be drawn that oil storage in depleted petroleum reservoirs is a feasible concept. To ensure the successful field implementation, the porosity, permeability, and non-uniformity of the reservoir are the primary criteria for candidate screening. In general, the favorable candidate should have a porosity of no less than 10%, a permeability of no less than 150 mD, and minimizes any fractures or high-permeability channels. A high injection pressure that is no more than breakdown pressure can maximize the storage capacity. During the withdrawal period, it may employ artificial lift techniques to boost the stored oil production.

CRediT authorship contribution statement

Xinrui Zhao: Data curation, Writing - original draft. **Ridha Al-Abdrabalnabi:** Investigation, Visualization. **Yu-Shu Wu:** Conceptualization, Methodology, Supervision. **Xianmin Zhou:** Validation, Resources, Writing - review & editing.

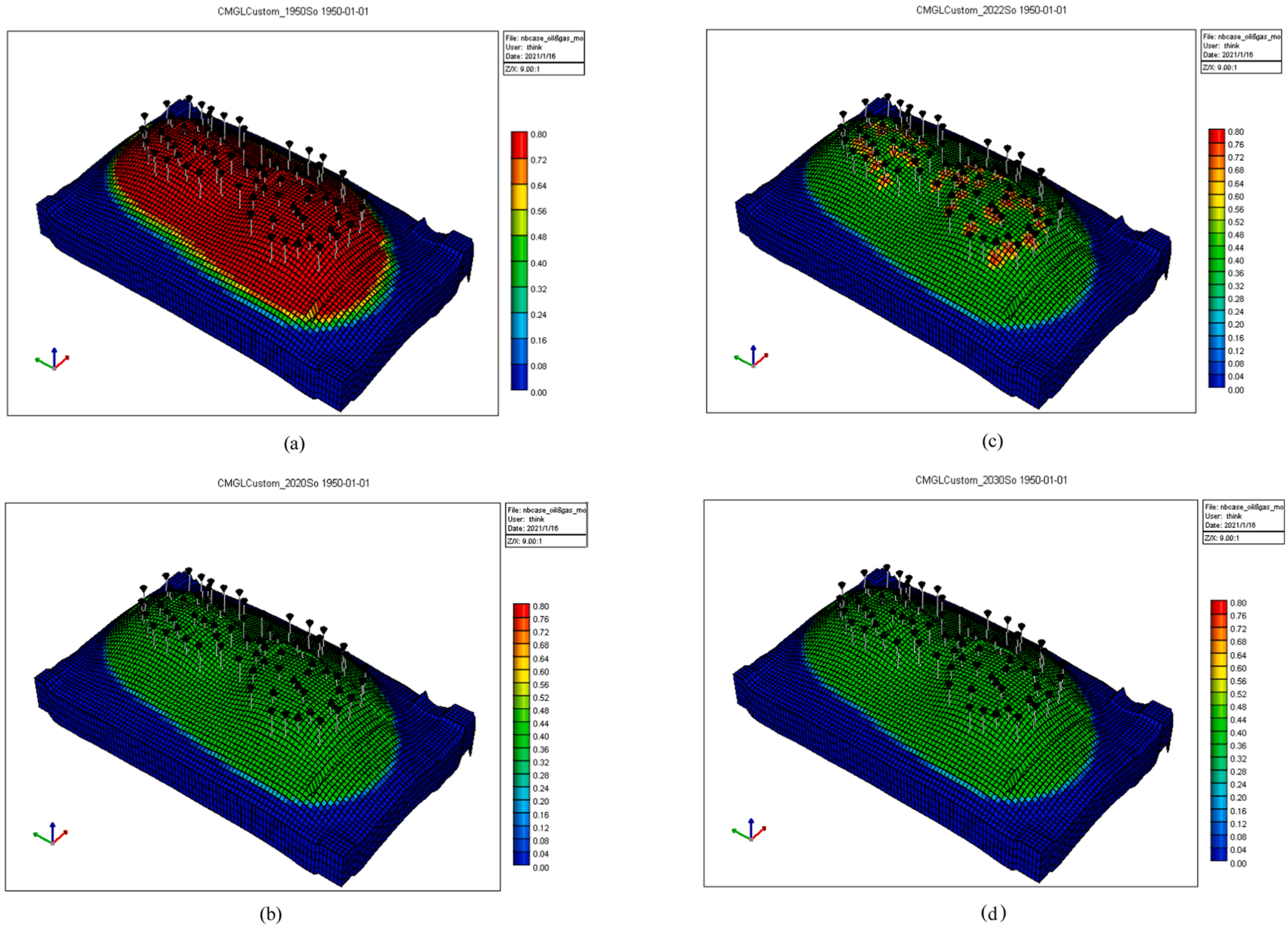

Fig. 19. The oil saturation profile of the reservoir at initial state (a), the end of first water flooding (b), the oil injection (c), and second water flooding (d).

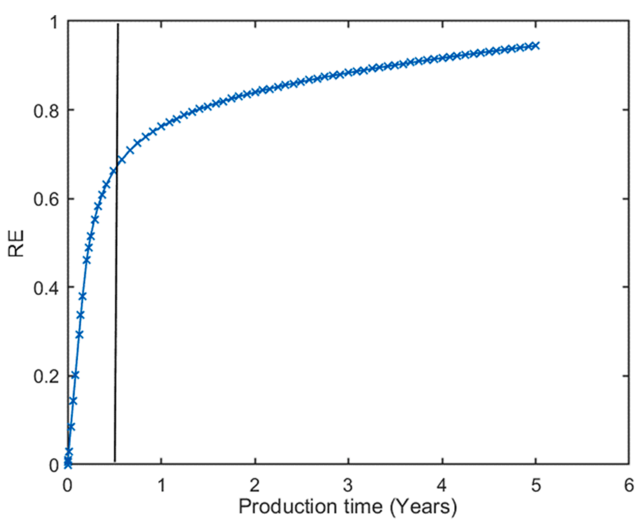

Fig. 20. Recovery efficiency of the stored dead crude oil vs. production time.

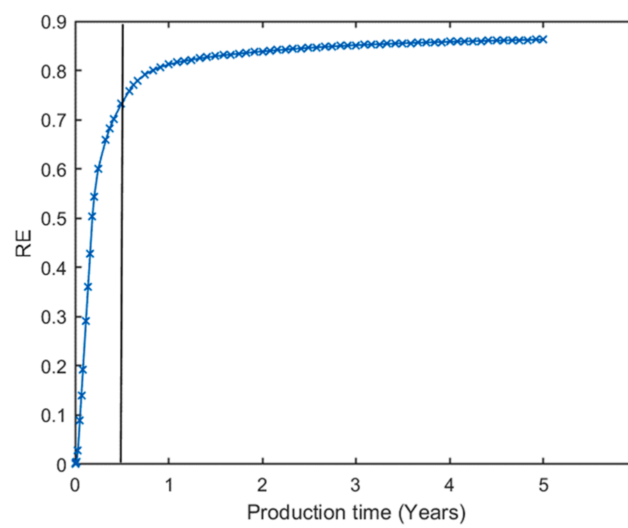

Fig. 21. Recovery efficiency of the stored live crude oil vs. production time.

Declaration of Competing Interest

The authors declare that they have no known competing financial interests or personal relationships that could have appeared to influence the work reported in this paper.

References

[1] Chang JI, Lin CC. A study of storage tank accidents. J Loss Prev Process Ind 2006; 19:51–9. https://doi.org/10.1016/j.jlp.2005.05.015.

[2] Rahimi M, Parvareh A. CFD study on mixing by coupled jet-impeller mixers in a large crude oil storage tank. Comput Chem Eng 2007;31:737–44. https://doi.org/10.1016/j.compchemeng.2006.07.009.

[3] Zhang N, Ma L, Wang M, Zhang Q, Li J, Fan P. Comprehensive risk evaluation of underground energy storage caverns in bedded rock salt. J Loss Prev Process Ind 2017;45:264–76. https://doi.org/10.1016/j.jlp.2016.10.016.
[4] Uliasz-Misiak B, Przybycin A. Present and future status of the underground space use in Poland. Environ Earth Sci 2016;75:1–15. https://doi.org/10.1007/s12665-016-6227-8.
[5] Ying J, Wenbo L. Research on China's renewable energy strategic development strategy from the perspective of sustainable development. IOP Conf. Ser. Earth Environ. Sci., vol. 510, Institute of Physics Publishing; 2020, p. 32026. doi: 10.1088/1755-1315/510/3/032026.
[6] Lucas D, Littlejohn D, Orlando E, Lindsey RP. The heavy oil storage tank project. Soc. Pet. Eng. - SPE/EPA Explore. Prod. Environ. Conf. 1997, EPEC 1997, Society of Petroleum Engineers; 1997. doi: 10.2118/37886-ms.
[7] Li Y, Chen YF, Zhang GJ, Liu Y, Zhou CB. A numerical procedure for modeling the seepage field of water-sealed underground oil and gas storage caverns. Tunn Undergr Sp Technol 2017;66:56–63. https://doi.org/10.1016/j.tust.2017.04.002.
[8] Tarasenko A, Chepur P, Gruchenkova A. Study of Deformations in a Large-Capacity Oil Storage Tank in the Presence of Subgrade Inhomogeneity Zones. MATEC Web Conf., vol. 73, EDP Sciences; 2016, p. 01025. doi: 10.1051/matecconf/20167301025.
[9] Brossia CS, Qu D, Qi B. Corrosion Monitoring of Oil Storage Tanks. NACE International; 2019.
[10] Liu W, Zhou Q, Li L, Wu Z, Cao F, Gao Z. Effect of alloy element on corrosion behavior of the huge crude oil storage tank steel in seawater. J Alloys Compd 2014;598:198–204. https://doi.org/10.1016/j.jallcom.2014.01.181.
[11] Mortazavi A, Nasab H. Analysis of the behavior of large underground oil storage caverns in salt rock. Int J Numer Anal Methods Geomech 2017;41:602–24. https://doi.org/10.1002/nag.2576.
[12] Ma K, Tang CA, Wang LX, Tang DH, Zhuang DY, Zhang QB, et al. Stability analysis of underground oil storage caverns by an integrated numerical and microseismic monitoring approach. Tunn Undergr Sp Technol 2016;54:81–91. https://doi.org/10.1016/j.tust.2016.01.024.
[13] Kiyoyama S. The present state of underground crude oil storage technology in Japan. Tunn Undergr Sp Technol Inc Trenchless 1990;5:343–9. https://doi.org/10.1016/0886-7798(90)90129-8.
[14] Katz DL, Tek MR. Overview on underground storage of natural gas. JPT, J Pet Technol 1981;33:943–51. https://doi.org/10.2118/9390-PA.
[15] Azin R, Nasiri A, Entezari J. Underground gas storage in a partially depleted gas reservoir. Oil Gas Sci Technol - Rev l'IFP 2008;63:691–703. https://doi.org/10.2516/ogst:2008028.
[16] Favret F. Up-to-date researches and future trends in underground gas storage facillties: a state of the art review. Secur. Nat. Gas Supply through Transit Ctries., Kluwer Academic Publishers; 2006, p. 159–93. doi: 10.1007/1-4020-2078-3_8.
[17] Zheng D, Xu H, Wang J, Sun J, Zhao K, Li C, et al. Key evaluation techniques in the process of gas reservoir being converted into underground gas storage. Pet Explor Dev 2017;44:840–9. https://doi.org/10.1016/S1876-3804(17)30095-2.
[18] Teatini P, Castelletto N, Ferronato M, Gambolati G, Janna C, Cairo E, et al. Geomechanical response to seasonal gas storage in depleted reservoirs: a case study in the Po River basin, Italy. J Geophys Res Earth Surf 2011;116. https://doi.org/10.1029/2010JF001793.
[19] Dharmananda K, Kingsbury N, Singh H. Underground Gas Storage: Issues Beneath the Surface, Society of Petroleum Engineers (SPE); 2004. doi: 10.2118/88491-ms.
[20] Aladasani A, Bai B, Wu Y-S, Okasha Q. 3D simulation of low salinity, polymer, conventional, water-flooding; combination IOR methods – heterogeneous; varying wetting conditions. SPE/IATMI Asia Pacific Oil Gas Conf. Exhib., Society of Petroleum Engineers; 2015. doi: 10.2118/176315-MS.
[21] [21] Tureyen OI, Karaalioglu H, Satman A. Effect of the wellbore conditions on the performance of underground gas-storage reservoirs. Soc. Pet. Eng. - SPE/CERI Gas Technol. Symp. 2000, GTS 2000, Society of Petroleum Engineers; 2000. doi: 10.2118/59737-ms.
[22] Zhou X, Morrow NR, Ma S. Interrelationship of wettability, initial water saturation, aging time, and oil recovery by spontaneous imbibition and waterflooding. SPE J 2000;5:199–207. https://doi.org/10.2118/62507-PA.
[23] Corey AT. The interrelation between gas and oil relative permeabilities. Producers Monthly 1954 Nov;19(1):38–41.
[24] Zhou X, Al-Otaibi F, Kokal S. Relative permeability characteristics and wetting behavior of supercritical CO2 displacing water and remaining oil for carbonate rocks at reservoir conditions. Energy Fuels 2019;33:5464–75. https://doi.org/10.1021/acs.energyfuels.9b01053.
[25] Jha B, Bottazzi F, Wojcik R, Coccia M, Bechor N, McLaughlin D, et al. Reservoir characterization in an underground gas storage field using joint inversion of flow and geodetic data. Int J Numer Anal Methods Geomech 2015;39:1619–38. https://doi.org/10.1002/nag.2427.
[26] Sakhaee-Pour A, Agrawal A. Predicting breakdown pressure and breakdown cycle in cyclic fracturing. SPE Prod Oper 2018;33:761–9. https://doi.org/10.2118/191137-PA.